ACS APPLIED MATERIALS & INTERFACES

Research Article

www.acsami.org

Surface Morphology-Dependent Room-Temperature $LaFeO_3$ Nanostructure Thin Films as Selective NO_2 Gas Sensor Prepared by Radio Frequency Magnetron Sputtering

S. Thirumalairajan,*[,†,‡] K. Girija,[‡,§] Valmor R. Mastelaro,[†] and N. Ponpandian[‡]

[†]Instituto de Física de São Carlos (IFSC), University de São Paulo, CP 369, 13560-970 São Carlos, SP, Brazil

[‡]Department of Nanoscience and Technology, Bharathiar University, Coimbatore-641 046, India

[§] Department of Science and Humanities, Dr. N.G.P. Institute of Technology, Coimbatore-641 048, India

ABSTRACT: In the present work, perovskite $LaFeO_3$ thin films with unique morphology were obtained on silicon substrate using radio frequency magnetron sputtering technique. The effect of thickness and temperature on the morphological and structural properties of $LaFeO_3$ films was systematically studied. The X-ray diffraction pattern explored the highly oriented orthorhombic perovskite phase of the prepared thin films along [121]. Electron micrograph images exposed the network and nanocube surface morphology of $LaFeO_3$ thin films with average sizes of ∼90 and 70 nm, respectively. The developed $LaFeO_3$ thin films not only possess unique morphology, but also influence the gas-sensing performance toward NO_2. Among the two morphologies, nanocubes exhibited high sensitivity, good selectivity, fast response−recovery time, and excellent repeatability for 1 ppm level of NO_2 gas at room temperature. The response time for nanocubes was 24−11 s with a recovery duration of 35−15 s less than the network structure. The sensitivity toward NO_2 detection was found to be in the range 29.60−157.89. The enhancement in gas-sensing properties is attributed to their porous structure, surface morphology, numerous surface active sites, and the oxygen vacancies. The gas-sensing measurements demonstrate that the $LaFeO_3$ sensing material is an outstanding candidate for NO_2 detection.

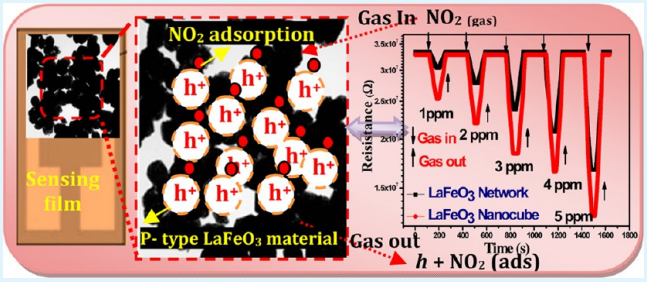

KEYWORDS: *$LaFeO_3$, thin films, network, nanocubes, radio frequency sputtering, NO_2 gas*

1. INTRODUCTION

Sensor applications widely encompass environmental monitoring, fire detection, safety measures, food quality control, and many other relevant areas.[1−3] In particular, the development of advanced automotive propulsion systems employing new materials, designs, and fuels requires the continuous monitoring of exhaust gases. While monitoring the oxygen content is the primary method of optimizing the combustion process, emission control requires the monitoring of toxic gases such as NO_2, CO, O_3, etc.[4] Among them, nitrogen dioxide (NO_2) is one of the most toxic air pollutants and is the main source of acid rain, photochemical smog that is harmful to humans, animals, and plants.[5−7] It becomes a cause of concern when one is over exposed (lower tolerance limit ∼5 ppm) as it may lead to pulmonary disease and in extreme cases even the loss of human life.[8] Therefore, NO_2 sensor with high-sensitivity, good selectivity, fast response−recovery time, excellent stability, and that can be operated at room temperature has become increasingly significant to human health and environment protection.[9] Nanomaterials offer the opening to dramatically increase the response to NO_2 toxic gas, as their performance is directly related to the exposed surface volume. Perovskite oxide (ABO_3, where position A is occupied by a rare earth ion, and B by the transition metal ion) materials are involved in the effort to enhance the performance of the detection of combustible and toxic gases at low-cost. A number of perovskite oxides have been proposed earlier as gas sensor material because of their stability even at high temperature and in a chemically aggressive atmosphere.[10] Many perovskites show p-type semiconducting behavior in air. Oxygen adsorption enhances the conductivity of these materials because of the increased concentration of holes, which are the main charge carrier species.[11−14] $LaFeO_3$ is one of the p-type semiconductors having high electrical conductivity and exhibits good oxidation−reduction characteristics at wide temperature and good matched properties for sensing.[15] Hence, $LaFeO_3$ was chosen as a sensing material to sense oxidation gas (NO_2) in the present work. In addition, the morphology and structure of $LaFeO_3$ material is the key factor in influencing the performance and enhancing the gas-sensing properties. However, controlling the morphology and particle size of perovskite materials is not simple.[16,17] Considerable interests have been developed for the preparation of perovskite oxides

Received: May 27, 2014
Accepted: July 16, 2014
Published: July 16, 2014

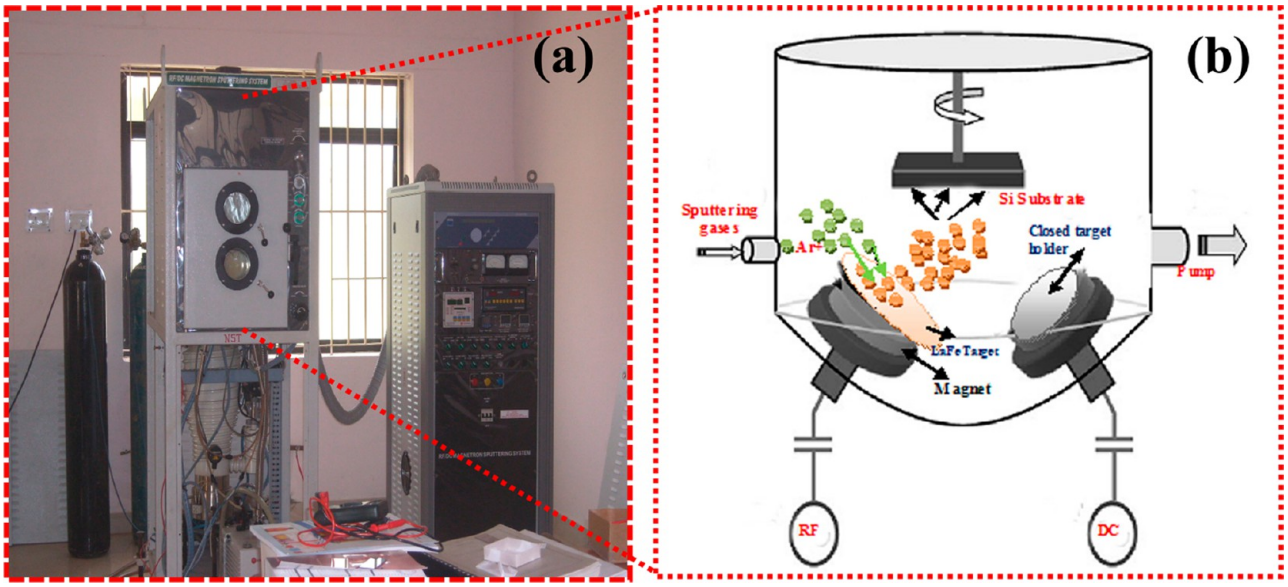

Figure 1. (a) Photograph of RF/DC reactive magnetron sputtering unit, and (b) schematic diagram of the process taking place within the chamber.

possessing unique morphology and enhanced properties through novel methods for its potential application as a gas sensor.[18] Moreover, in the case of practical applications, the main challenge consists of finding cost-effective and scalable preparation methods for the production of these nanostructured perovskite materials.[19] Among the many physical techniques available, sputtering is a well renowned technique for the fabrication of thin films of materials with very high melting point such as zinc, cobalt, and alloy compounds, which cannot be easily melted to induce self-catalytic growth of their oxides.[20−23] On this basis, device fabrication and gas-sensing investigation of perovskite oxide nanostructures by physical techniques are more suited as compared to the chemical processes. Recently, research activities involving room-temperature NO_2 sensors like In_2O_3 nanowires, SnO_2, TiO_2, graphene, etc., fabricated through various techniques like laser ablation, nanopatterned CVD, electronspun, and chemical solution deposition have been reported. The detection limit of the sensor response ranges from below 1 ppb to 650 ppm.[24−28] There is still much scope in the studies of sensors fabricated with different morphology to understand the sensing phenomenon taking place with interaction of gases and the realization of the sensor structure exhibiting enhanced response characteristics. However, to the best of our knowledge, the detection of low level NO_2 gas at room temperature by $LaFeO_3$ thin films with different nanostructured morphology has not been explored in open literature.

In the present work, for the first time we report the deposition of $LaFeO_3$ nanostructure thin films with different morphologies by RF sputtering technique. To optimize the different morphologies obtained on the surface of the thin films, various operating parameters have been tuned and discussed in detail. The fabricated sensing device consisting of $LaFeO_3$ nanostructure thin films exhibited good sensing performance at room temperature for 1 ppm level of NO_2 gas. The built $LaFeO_3$ sensor possesses good sensitivity, selectivity, stability, and reproducibility toward the sensing performance.

2. EXPERIMENTAL PROCEDURE

Fabrication of $LaFeO_3$ Thin Films. For the deposition, pure lanthanum iron (LaFe) alloy 99.99% (Sigma-Aldrich) with 2 in. diameter and 2 mm thickness was used as the sputtering target. The films were sputtered onto silicon substrate at a deposition rate of 0.085 nm s^{-1}, and the photograph of RF/DC magnetron sputtering unit along with schematic illustration has been presented in Figure 1. The substrates were cleaned and spin dried before being loaded for deposition with a target to substrate distance of 10 cm. The RF power and the total pressure during deposition were 150 W and 5 mTorr, respectively. The initial base pressure was 2.5×10^{-6} mbar, which was raised to 7.2×10^{-2} mbar when the chamber was purged with high-purity argon and oxygen gas. Various samples were prepared by varying the film thickness (100, 200, 400, 600, and 800 nm) and the substrate temperature (room temperature (RT), 150, and 350 °C). Finally, the $LaFeO_3$ thin films were annealed in air at 800 °C for 2 h to attain their thermal stabilization in view of functional tests. Both argon and oxygen flow were controlled by mass flow controllers and allowed into the chamber at 50 sccm with gas in the ratio 10:1. Argon was used as the sputtering gas, while oxygen was used as the reactive gas. Before deposition, a presputtering process was employed to clean the target surface. The thickness of the deposited film was measured by a Tencor Alpha-step profiler. The deposition conditions were varied, and the best condition for preparing different nanostructure thin films was optimized.

Film Characterization and Property Measurements. The products obtained at various stages of preparation were taken out for systematic characterization to understand the growth of $LaFeO_3$ thin films using different analytical techniques. The surface roughness, morphology, structure, and compositional analysis of the prepared films were characterized using atomic force microscopy (AFM, Veeco dicaliber high value scanning probe microscope), scanning electron microscopy (SEM, JEOL JSM-6380LV), transmission electron microscopy (TEM, JEM 2100 F) performed with an acceleration voltage of 200 kV by placing the powder on a copper grid, and X-ray diffraction (XRD, Bruker Germany D8 Advance) with Cu $K_{\alpha 1}$ radiation (λ = 1.54 Å), and X-ray photoelectron spectroscopy (XPS) measurements were performed on an ESCA + Omicron UK XPS system with Mg Kα source and photon energy 1486.6 eV. All of the binding energies were referenced to the C 1s peak at 284.6 eV of the surface adventitious carbon.

Gas Sensor System and Measurement. The sensing characteristics of p-type $LaFeO_3$ thin film were examined using a home-built testing chamber. Electrical contacts were developed over the film

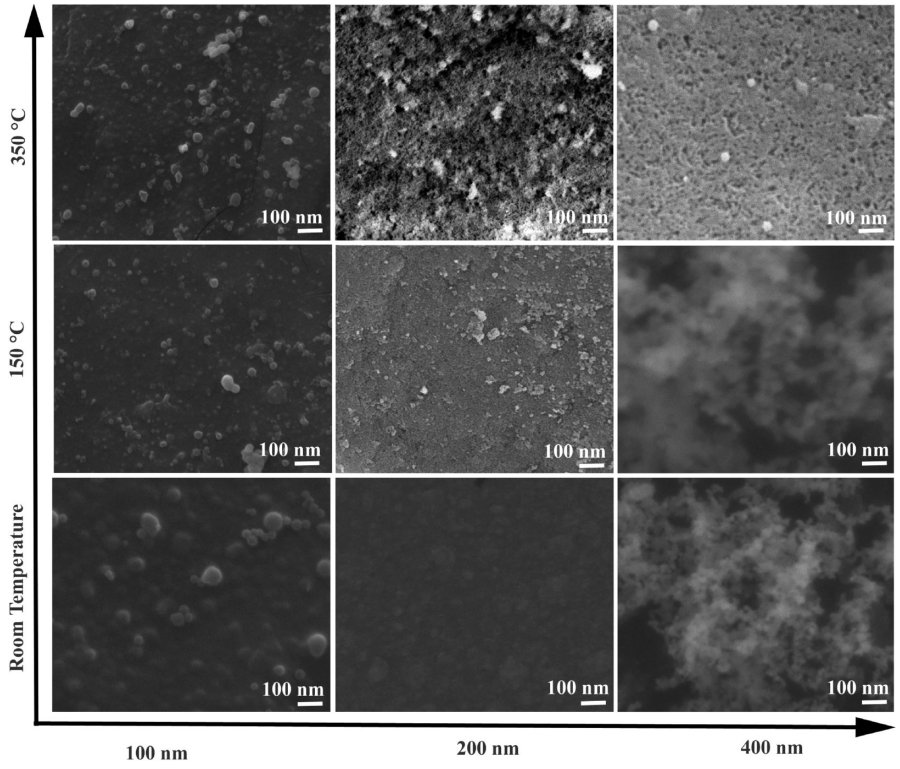

Figure 2. SEM images of $LaFeO_3$ samples with different thicknesses and deposition temperatures.

surface area of 12 mm × 10 mm using thin copper wire and highly conducting silver paste. The ceramic tube containing the sample was then placed inside the furnace maintained at the required temperature controlled with a PID temperature controller. The dry synthetic air with sample gas was flowed at 100 mL/min. Both electrodes were exposed to the same gas environment. The change in oxide ion pumping current was measured by the dc two-probe method. In the amperometric mode, dc 1 V was applied using a potentiostat/galvanostat (Hokuto Denko, HA301) as the active electrode and a positive one. The current was measured with a digital electrometer (Advantest, model R8240). The p-type $LaFeO_3$ was used to sense the oxidizing gas NO_2 whose response is defined as $S = R_{air}/R_{gas}$, where S is defined as the ratio of the resistance in the air (R_{air}) and the sensor resistance was measured when exposed to the target oxidizing gas (R_{gas}). The changes in electrical resistance of the film during the process of injection and venting of NO_2 vapor were monitored using a LabVIEW controlled data acquisition system. The gas sensor measurements were performed in the range from 25 (room temperature) to 100 °C. The sensor test devices were equilibrated in dry air for 12 h at each temperature before the beginning of sensor measurement to ensure stable and reproducible baseline resistance. During the measurements, the humidity was under controlled condition within the range 40−50% RH.

3. RESULTS AND DISCUSSION

3.1. Effect of Thickness and Substrate Temperature on the $LaFeO_3$ Thin Films. *3.1.1. Morphological Analysis.* The films were prepared with the aim of obtaining morphologies desirable for electrical properties and further use in gas-sensing application. Films with different thicknesses such as 100, 200, and 400 nm were deposited on cleaned silicon substrate at various deposition temperatures like RT, 150, and 350 °C. These films were examined using scanning electron microscopy to identify the surface morphology. The SEM image of all of these samples shows surfaces with no interesting morphologies as in Figure 2.

The sample deposited at lower thickness (100 nm) hardly shows any morphology on its surface at all of the temperatures. However, when the films were deposited at 200 and 400 nm, respectively, at 350 °C tiny clusters of agglomerated structures can be observed, giving a scope for defined morphologies at higher thickness.

Upon increasing the film thickness to 600 nm at 350 °C, the tiny agglomerated structures began to grow upward and finally were connected with each other to form network-like structures, and the interconnected structures have an average diameter of ∼90 nm as observed in Figure 3a. On further increasing the thickness to 800 nm at 350 °C, it was found that more $LaFeO_3$ nanoparticles were deposited on the surface, which self-assembled to form $LaFeO_3$ nanocubes (Figure 3b) with average particle size ∼70 nm. It is clearly observed that the nanocubes are tightly packed, which may be attributed to the increase in film thickness. On the other hand, when the substrate temperature was 150 °C with film thickness 600 nm, formation of network-like structures on the surface of the sample can be observed along with a few agglomerated nanoparticles as shown in Figure 3c. Similarly, the onset of nanocube formation was initiated above 150 °C with film thickness of 800 nm (Figure 3d). The particles are agglomerated and tempted to self-assemble to form nanocubes. No interesting morphology was evidenced at RT for film thicknesses of 600 and 800 nm (Figure 3e and f). Variation in surface morphology can be observed with increase in deposition temperature and film thickness. No change in surface morphology was detected by further increasing the thickness to 1000 nm. When the substrate temperature and thickness increase, the mobility of the atoms adsorbed on the surface of the film increases, and they diffuse into a more energetically favored site such as the interstitial positions, voids,

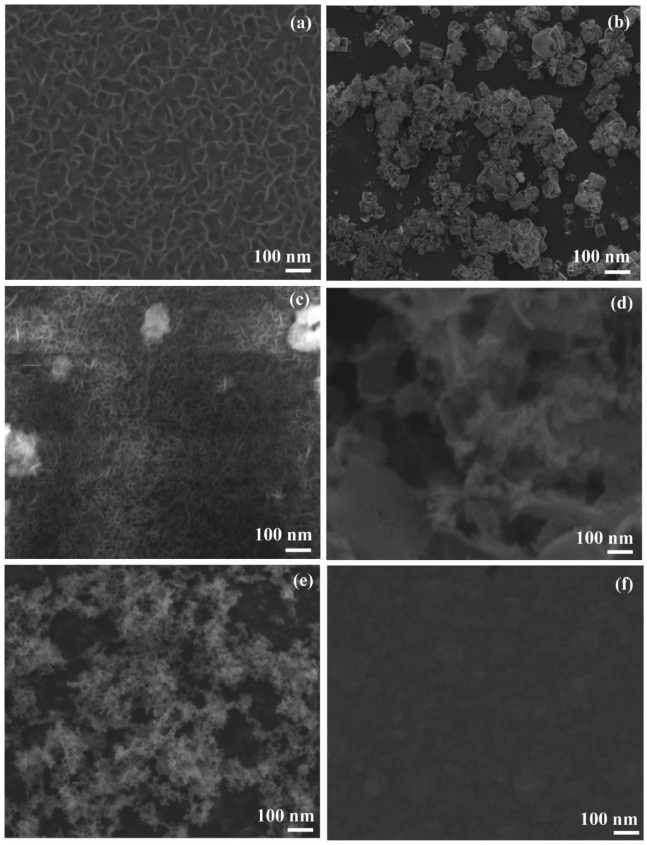

Figure 3. SEM images of different $LaFeO_3$ nanostructures deposited at substrate temperatures of (a) 350 °C, (c) 150 °C, (e) RT for network structures (thickness 600 nm), and (b) 350 °C, (d) 150 °C, (f) RT for nanocubes (thickness 800 nm).

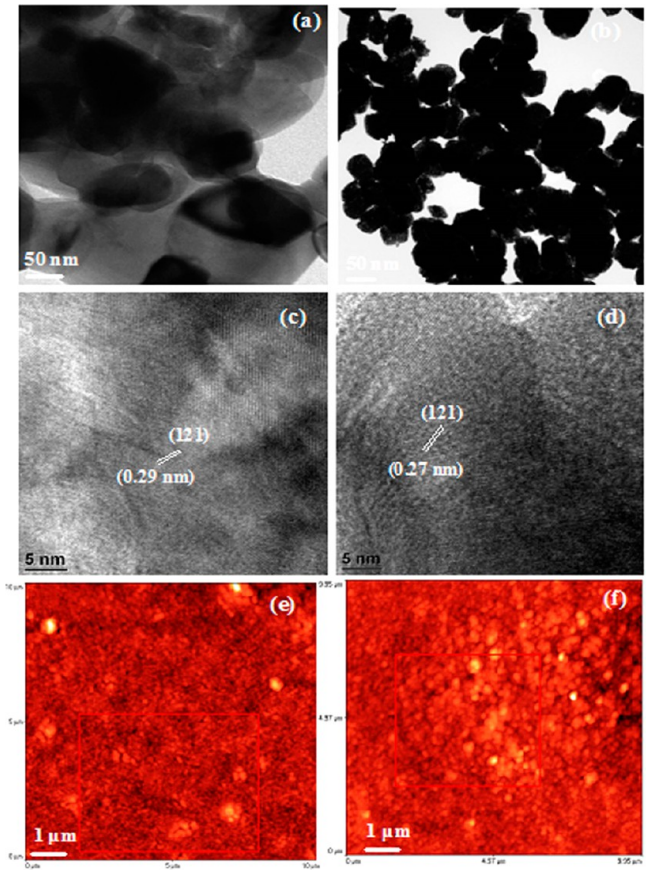

Figure 4. TEM (a and b), HRTEM (c and d), and AFM images (e and f) of network and nanocube $LaFeO_3$ thin films.

and grain boundaries, and subsequently the film porosity decreases.[29]

The above results indicate that the substrate temperature and film thickness is an important parameter for the formation of clear and well-defined morphology. On comparing the samples prepared with different film thicknesses and temperatures, it can be concluded that the films with thicknesses of 600 and 800 nm deposited at 350 °C as shown in Figure 3a and b have clear and interesting nanostructure morphology; hence, these samples were used for the TEM, AFM analysis and for sensing measurements.

The TEM and high-resolution TEM (HRTEM) images of the $LaFeO_3$ network and nanocube thin films and the corresponding AFM images of the samples are shown in Figure 4a–f. A close observation of network and nanocube structures (Figure 4a and b) clearly confirms the average size to be ∼90 and 70 nm. The alternate bright and dark regions signify the variations in the surface thickness of the $LaFeO_3$ nanostructure thin films with pores on its surface. The HRTEM image (Figure 4c and d) taken at the tip portion of the network and nanocubes exhibits the lattice planes with interplanar spacing of d_{121} = 0.29 nm for network and d_{121} = 0.27 nm for nanocube structures corresponding to the [121] direction of $LaFeO_3$ thin films. Further, insight on the surface roughness of the different $LaFeO_3$ nanostructure thin films was studied using atomic force microscopy. The topographical images of the surface of $LaFeO_3$ nanostructure thin films were obtained at five different locations, and the average RMS roughness and grain size values were determined. Figure 4e shows the 2D representation from which it is inferred that the network structures have a random arrangement along the surface of the substrate. The morphology has an interconnected porous network. The average depth of each pore-like appearance held between network structures is ∼86.88 nm with RMS roughness 8.13 nm, and the well-defined grain boundaries are also observed within the scanning area. Figure 4f represents the surface topography recorded for the nanocube $LaFeO_3$ thin film, which shows the formation of cube structure with grain size ∼72.48 nm and RMS roughness value ∼8.05 nm. A dense growth of the nanocubes was observed all over the surface forming a bunch of small grains. The overall growth appears more homogeneous at this stage, and also the surface seems to have well-defined grain boundaries. According to the Van der Drift model,[30] the randomly orientated nuclei were developed at the initial stage of deposition followed by the growth of nanocrystals. Finally, crystals with higher vertical growth rate might have a greater probability for survival, and as a result small and well oriented grains can be obtained. When the mean free path of free charge carriers is comparable with the dimension of the grains, the surface influence on the charge mobility becomes dominant.[31] Thus, the gas-sensing properties are based on the surface reactions between the sensing material and the test gas. Surface roughness is directly proportional to the gas sensitivity of the film because larger roughness results in larger contact area with the gaseous species. This demonstrates the importance of the surface-to-volume ratio in gas-sensing application.[32]

3.1.2. Structural Analysis. The powder XRD pattern provides crystallinity and phase information for the prepared

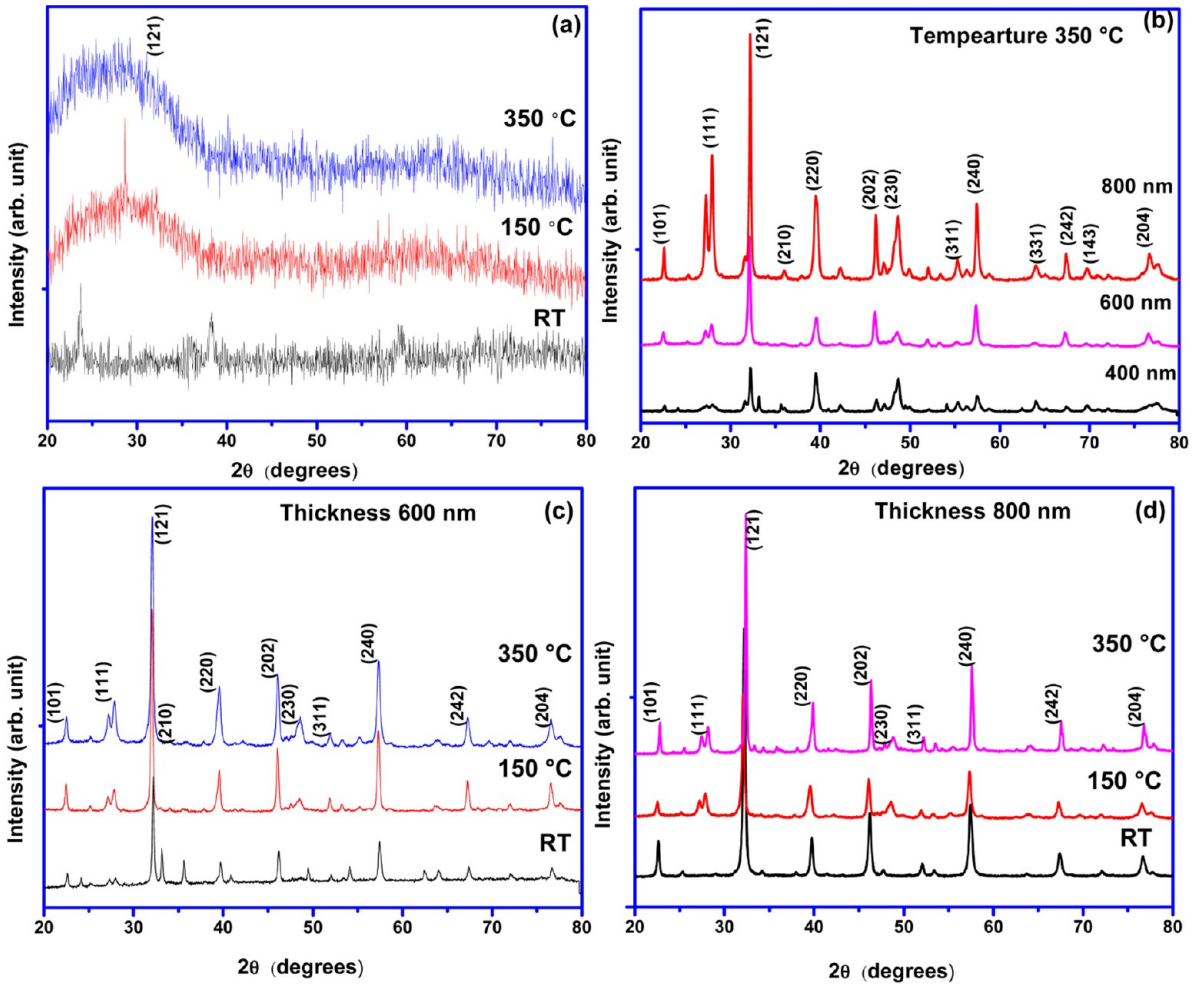

Figure 5. (a) XRD pattern of 200 nm thick samples deposited at different substrate temperatures, (b) different thicknesses, (c) various substrate temperatures of network, and (d) various substrate temperatures of nanocubes.

samples. The XRD patterns of the samples deposited with different thicknesses and substrate temperatures are shown in Figure 5. The sample deposited at room temperature shows impurity peaks and is amorphous in nature as shown in Figure 5a for 200 nm thickness. The XRD pattern of sample deposited at 150 °C exhibits few peaks, indicating the growth of the crystallites along the (121) plane. For the sample deposited with substrate temperature 350 °C, diffraction peaks with increased intensity were observed. It can be clearly envisaged that as the substrate temperature increases, the oriented growth of crystallites along (121) plane increases. Further, the XRD patterns of $LaFeO_3$ samples with different thicknesses of 400, 600, and 800 nm at 350 °C are presented in Figure 5b. The XRD peaks are well-defined, and it indicates the samples prepared under various thicknesses are well crystallized. The XRD patterns for $LaFeO_3$ network and nanocube thin films at substrate temperatures of RT, 150, and 350 °C, respectively, were also analyzed. The crystalline nature and the orientation of both nanostructures are shown in Figure 5c and d. The XRD patterns of all of the samples indicate that the crystalline films deposited are of perovskite phase with orthorhombic structure having a *Pnma* space group.[33] The lattice parameters estimated from the XRD pattern were found to lie in the range a = 5.5655−5.5659 Å, b = 7.8383−7.8389 Å, and c = 5.5776−5.5779 Å with a maximum experimental error of ±0.0003, which is in accordance with that of bulk $LaFeO_3$ crystal (JCPDS no. 37-1493).[34] The calculated average crystallite size for network structures is ∼89 nm and for nanocubes ∼71 nm at 350 °C, almost in agreement with the results obtained from the morphological analysis.

The above results confirmed that there is no significant change in the lattice parameters with the change in film thickness in the range 400−800 nm. Also, there are no peaks corresponding to La_2O_3/or Fe_2O_3, confirming the presence of single phase $LaFeO_3$. The XRD peak intensities of $LaFeO_3$ samples with the thickness of 400 nm are less when compared to those of 600 and 800 nm, which indicates the samples with higher thickness have higher crystallinity when compared to those with lower thickness. When the thickness is increased to 600 and 800 nm, the diffraction peaks turned sharper and stronger, which indicates the pure crystal quality of the resultant nanoparticles. The above results reveal that the thickness and substrate temperature play a vital role in controlling the growth of different $LaFeO_3$ nanostructures. Hence, single phase perovskite $LaFeO_3$ thin films with good crystalline quality and clear morphology as observed in Figure 3a and b at 350 °C were used for further characterization and gas-sensing measurements in the present study.

3.2. Composition Analysis. The surface elemental composition and chemical status of different $LaFeO_3$ nanostructure thin films were analyzed using the spectrum obtained from the X-ray photoelectron spectroscopy (XPS)

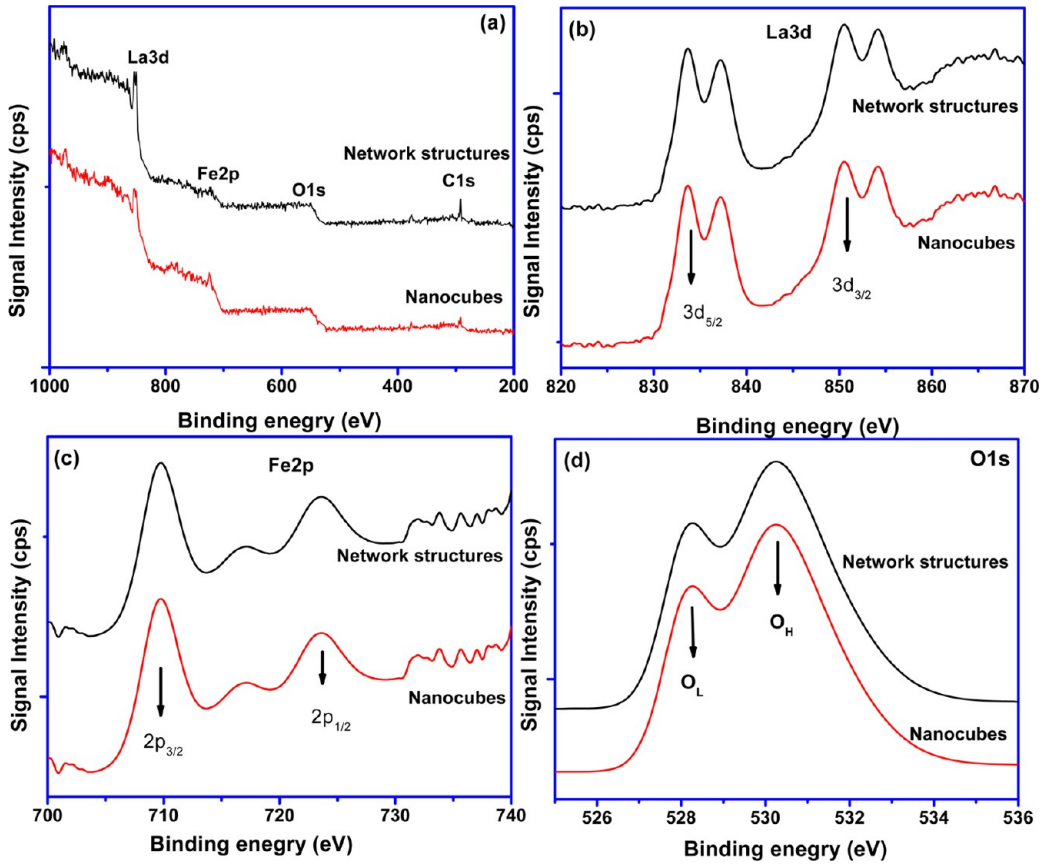

Figure 6. (a) XPS survey spectrum, (b) La 3d, (c) Fe 2p, and (d) O 1s spectra of network and nanocube $LaFeO_3$ thin films.

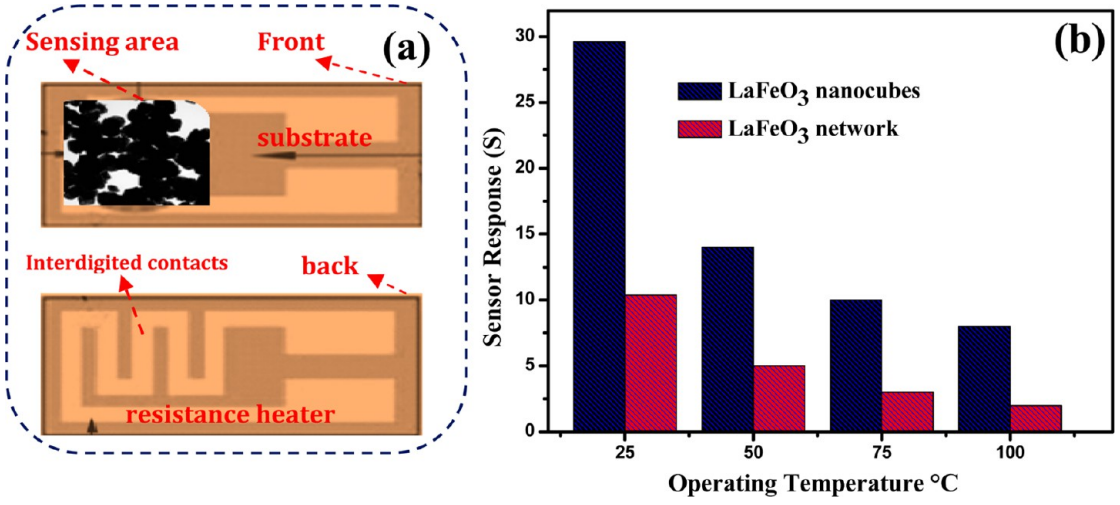

Figure 7. (a) Schematic diagram of the $LaFeO_3$ sensing film, and (b) the response to 1 ppm of NO_2 gas by the $LaFeO_3$ thin films working at different temperatures.

measurements. The binding energies obtained were corrected for specimen charging using C 1s as the reference at 284.6 eV. The typical XPS survey spectra obtained for network and nanocube morphology of $LaFeO_3$ are shown in Figure 6a, which reveals the presence of La(3d), Fe(2p), O(1s), and C(1s). The carbon peak can be attributed to the presence of adventitious carbon on the surface of the samples. The La 3d and Fe 2p core-level spectrum reveals that the lanthanum and iron atoms in the $LaFeO_3$ samples exist in the formal chemical valence state of +3.[35] The high-resolution spectrum in Figure 6b represents two strong La peaks at 833.12 and 850.29 eV for network structure and 833.66 and 850.72 eV for nanocubes, which corresponds to the spin−orbit splitting of $3d_{5/2}$ and $3d_{3/2}$ of La^{3+} ions in oxide form. The binding energies of Fe $2p_{3/2}$ and Fe $2p_{1/2}$ were observed at 709.2 and 723.53 eV for network structure and 709.36 and 725.84 eV for nanocubes as shown in Figure 6c, which corresponds to Fe^{3+} ions in oxide form. No peak due to Fe^{2+} can be found, which confirms that oxidation state of Fe is 3+ in $LaFeO_3$ nanostructure thin films.[36] The two O 1s XPS spectra in Figure 6d are wide and asymmetric,

demonstrating that there are at least two kinds of O chemical states according to the binding energy of network and nanocube structures at 528.36 and 528. 86 eV ascribed to the lattice oxygen species (OL) and 530.54 and 530. 86 eV assigned to the chemisorbed hydroxyl oxygen species. The O(1s) binding energy of O^- ions is higher by 2.1−2.5 eV than that of lattice oxygen.[37]

The binding energy of OL XPS signal can be attributed to the contribution of La−O and Fe−O in $LaFeO_3$ crystal lattice. From the relative intensities of the XPS spectrum, the compositional stoichiometry was calculated between La, Fe, and O, and it was found to be 1:1:3. This kind of metal−support interaction has been taken as an important factor in the gas-sensing mechanism.

3.3. Device Fabrication and NO_2 Gas-Sensing Measurement of $LaFeO_3$ Nanostructure Thin Films. The fabricated $LaFeO_3$ sensor (schematic diagram in Figure 7a) was placed inside the ceramic tube attached to a gas flow assembly and external electrical contacts. Different $LaFeO_3$ nanostructure films were measured in dry synthetic air as a function of the temperature in the range from 25 (room temperature) to 100 °C as shown in Figure 7b. The response and recovery time are defined as the time taken by the sensor to achieve 90% of the total resistance variation in the case of adsorption and desorption, respectively. The registered sensor response value was greater for nanocubes than the network structures, for all the temperatures. The sensor resistance was around 10^7 Ω for the network $LaFeO_3$ thin film samples, and the resistance decreased by raising the temperature due to the increase in carrier mobility. At 25 °C, the response was maximum, and it can be related to the adsorption/desorption of oxygen on the $LaFeO_3$ surface.

For the nanocube $LaFeO_3$ thin film samples, the response was noticeably higher with respect to network $LaFeO_3$ sample at all temperatures, which can be associated with their crystallite size, porous nature, and particle−particle interaction. Also, the working temperature of the sensor, which regulates the adsorption/desorption processes at equilibrium, and the competition for chemisorption between NO_2 and atmospheric oxygen for the same active surface sites play an important role in determining the specific interaction between NO_2 and the sensing material.[38] To determine the optimum operating temperature, the response of the sensor toward 1 ppm of NO_2 was examined as a function of room temperature. The response value decreased correspondingly as the working temperature raised, and the maximum sensing value was 29.60 for $LaFeO_3$ nanocubes and 10.04 for the $LaFeO_3$ network structure at 25 °C for 1 ppm of NO_2 with an error limit of ±0.01%. Therefore, we choose RT (25 °C) as our working temperature to proceed with further analysis.

Figure 8 shows the resistance measurement of the different $LaFeO_3$ nanostructure thin film sensors toward toxic gas NO_2 in the concentration range 1−5 ppm at RT. At the start of the sensing experiment, the film exposed to dry air atmosphere exhibited higher resistance due to the oxidation reaction between the film surface and oxygen molecules.

The test gas was then introduced into the testing chamber. When oxidizing molecules (NO_2) are adsorbed onto the p-type $LaFeO_3$ surface, accumulation of holes is formed in response, resulting in the decrease of sensor resistance followed by complete recovery of their initial value when clean air was fed into the chamber. Both of the structures show response to NO_2 gas. The resistance value varies as the concentration changes,

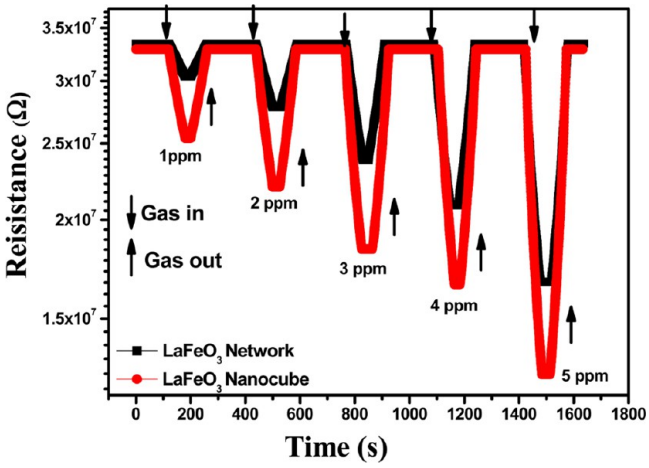

Figure 8. Transient sensing response of $LaFeO_3$ nanostructure thin films for different concentrations of NO_2 at RT.

and the curves exhibit a stepwise distribution. The $LaFeO_3$ nanocubes exhibit more response to NO_2 than the $LaFeO_3$ network structure.

Figure 9a shows the sensing response of $LaFeO_3$ network structures exposed to the oxidation gas at concentrations of 1−5 ppm of NO_2. A gradual increase in the sensor response was noticed on increasing the concentration of NO_2. The sensor response of $LaFeO_3$ network was observed in the range 10.03−100.33 for 1−5 ppm of NO_2 concentration. Further, Figure 9b shows the response of the sensing element with nanocube morphology on exposure to oxidization gas, and the sensitivity was found to increase with increase in gas concentration. The sensitivity values obtained by exposing the sensor to different concentration (1−5 ppm) of NO_2 were determined to be in the range 29.60−157.89, respectively. The analysis of sensing performance within an experimental error of ±0.01% demonstrates that the nanocube $LaFeO_3$ thin films show excellent catalytic activity upon exposure to NO_2 gas in comparison with $LaFeO_3$ network structure.

The sensing response of both the nanostructured films increased as the concentration increased, which is attributed to the number of oxygen-adsorption sites. The increase in response is ascribed to the fact that as the NO_2 concentration increases, more electrons will be liberated, thereby decreasing the electrical resistance. The electrical resistance of the film changed instantaneously, indicating the film showed a rapid response at room temperature. This might be due to the catalytic action of nanostructure $LaFeO_3$ thin films, which will enhance the reaction between chemisorbed oxygen ions and NO_2.[39] The sensitivity is highly dependent on film thickness, operating temperature, chemical composition, and crystallite size. Figure 9c and d represents the response and recovery time of $LaFeO_3$ nanostructure thin films of network and nanocube structures toward 1−5 ppm of NO_2 at RT with an experimental error of ±0.01%. The response time was found to be 24−11 s for nanocubes and 30−17 s for network. Consequently, the recovery time of $LaFeO_3$ network structure was 42−18 s and for the nanocube-based sensor 35 and 15 s for 1−5 ppm of NO_2 concentration. It was observed that with an increasing NO_2 concentration, the response and recovery time were quick at low concentration; more NO_2 molecules easily interact with adsorbed oxygen, providing a fast response. The observed fast response−recovery time (in the order of seconds) could be due

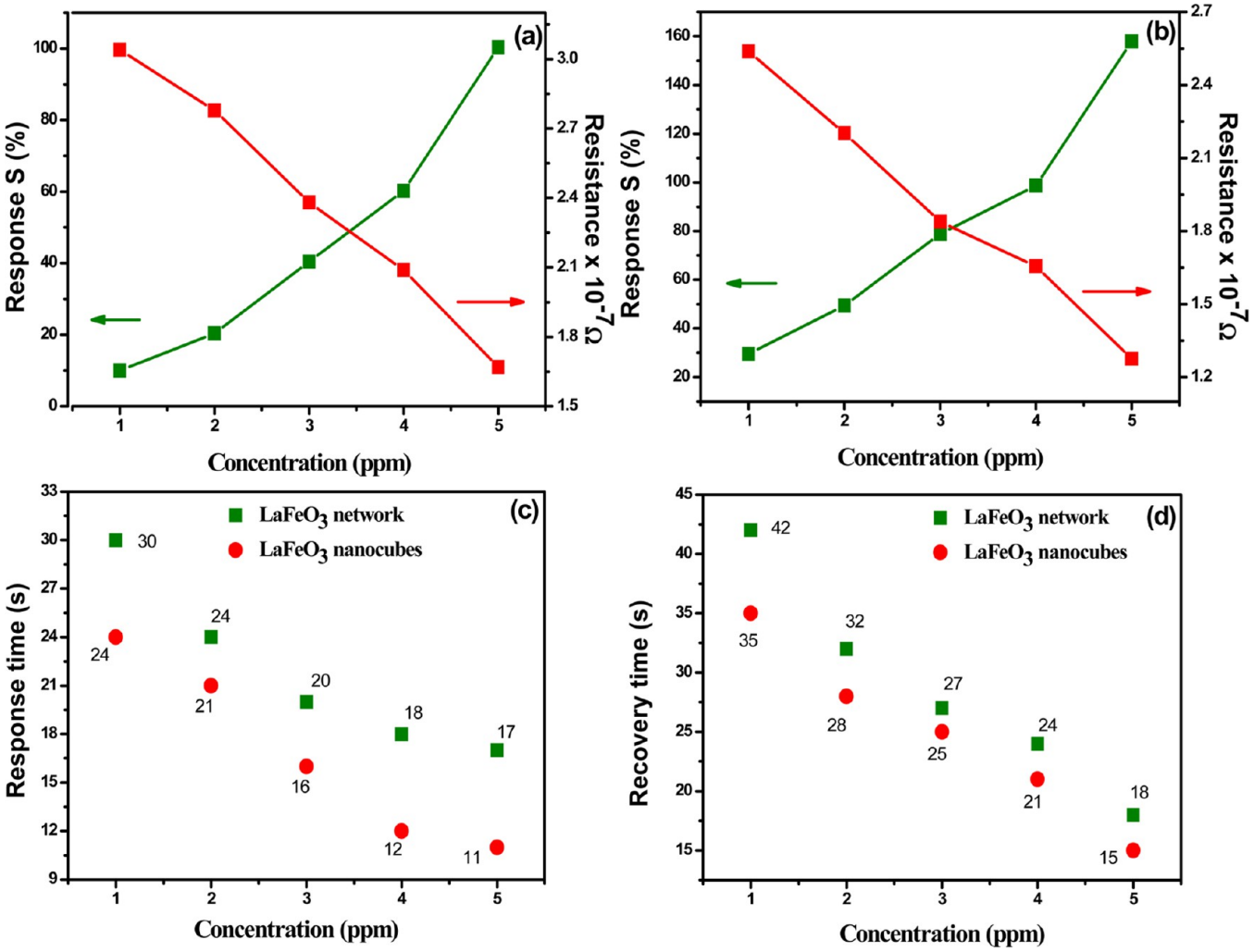

Figure 9. Sensing response and electrical resistance as a function of NO_2 concentration at RT: (a) $LaFeO_3$ network, (b) $LaFeO_3$ nanocubes, (c) response time (s), and (d) recovery time (s) of the statistical reports of different $LaFeO_3$ nanostructure thin films.

to the room-temperature operation, smaller grain size, and the nanostructured morphologies. The gas sensor performance in nanostructured materials is also highly sensitive to the BET surface area. The surface area of nanocubes and network structure was found to be 92.85 and 74.50 $m^2\ g^{-1}$, respectively. This could explain the higher sensor signal of the nanocubes versus network structure. The results clearly demonstrate the great advantage of nanocube $LaFeO_3$ thin films for real-time monitoring of NO_2 gas sensor.

Further, selectivity plays a major role in gas identification. The reduction and oxidization gases such as NO_2, O_2, CO, ammonia, acetone, and toluene have appreciable cross-sensitivity that hinders the development of a domestic gas sensor, which can distinguish these species as shown in Figure 10. The measurements were carried out for different concentrations of gases at RT, and the response for each vapor was recorded with an experimental error of ±0.01%. The film showed a comparatively lower response for toluene, acetone, ammonia, CO, and O_2. The reason for the high response to NO_2 can be due to the change in resistance for oxidizing gases, reaction with the adsorbed oxygen ions on the sensor surface, optimum porosity of the film, crystallite size, and catalytic activity of $LaFeO_3$ with NO_2 molecules. Moreover, electron acceptor ability of NO_2 is higher than that of other

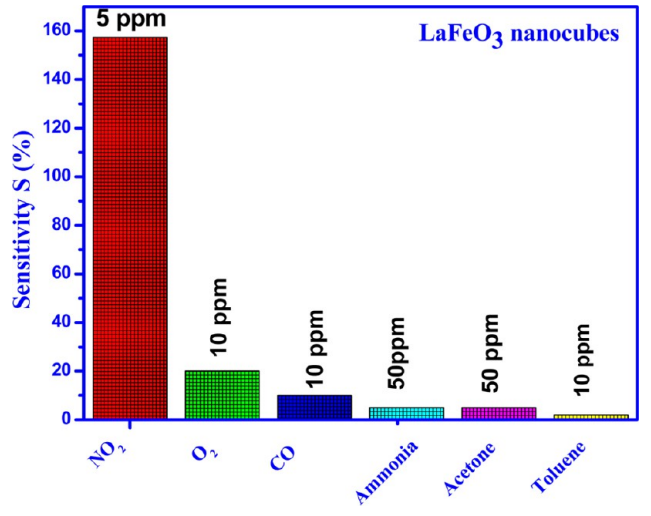

Figure 10. Sensing response of the $LaFeO_3$ thin films toward 5 ppm of NO_2 and other gases.

vapors because of the presence of lone pair of holes.[40−42] The fabricated gas sensor is practically insensitive to the other common interference gases, showing more selectivity toward NO_2 gas.

dx.doi.org/10.1021/am503318y | ACS Appl. Mater. Interfaces 2014, 6, 13917−13927

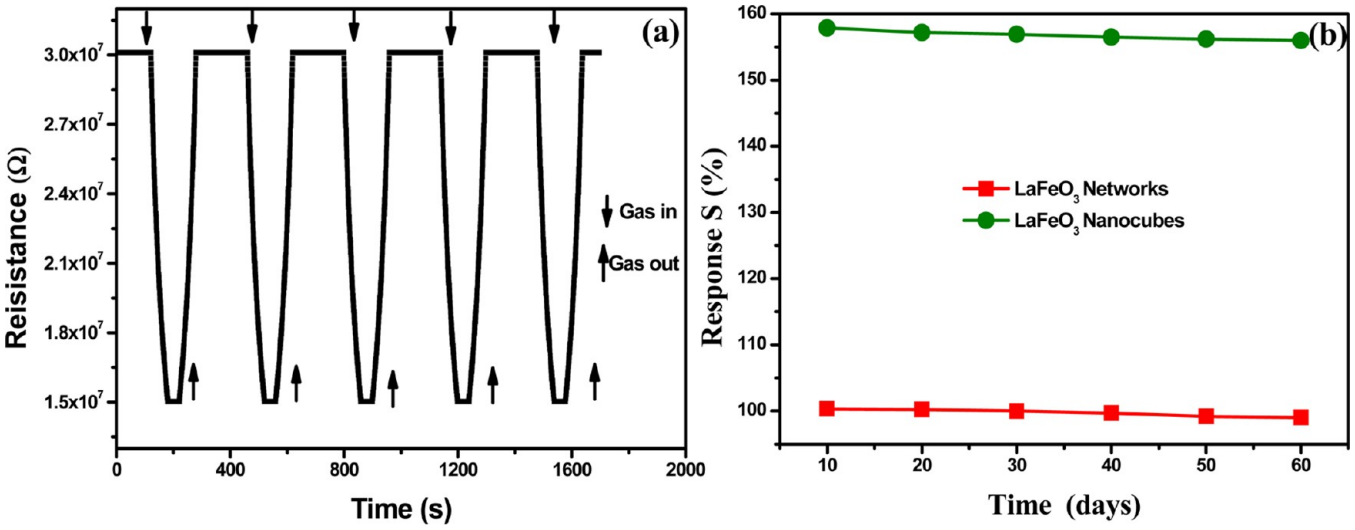

Figure 11. Reproducibility of NO_2 sensing response for 5 ppm (a) $LaFeO_3$ network, and (b) stability of different $LaFeO_3$ nanostructure thin film sensors at RT.

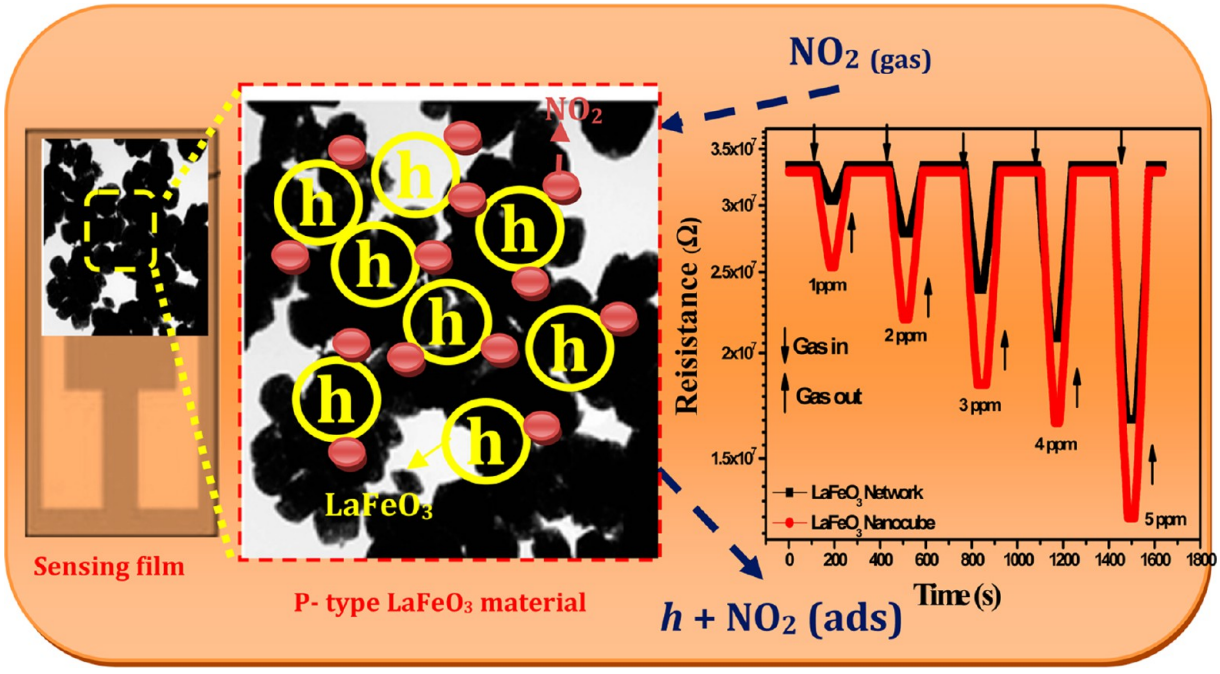

Figure 12. Schematic illustration of the hole accumulation space layer of $LaFeO_3$ nanostructure thin films toward oxidization gas NO_2.

The sensor response curves for five continuous gas in and out cycles of $LaFeO_3$ network thin films are shown in Figure 11a, which ascertains the reproducibility of the sensor response toward NO_2. After each gas in and out cycle, the sensor almost resorted to its initial value, which indicates the sensor has excellent repeatability. The sensing stability of the $LaFeO_3$ nanostructure thin films studied for 5 ppm of NO_2 at room temperature over a period of 60 days at intervals of 10 days is shown in Figure 11b. It was noticed that there exists a slight increase in the resistance baseline and subsequent decrease in the sensor response to NO_2 at an experimental error of ±0.01%. These studies were extended to film stored over a period of 2 months, which also confirm the good sensing stability of the $LaFeO_3$ nanostructure thin films. From the NO_2 sensor response curve, it can be evidenced that the $LaFeO_3$ nanocube structures show excellent sensitivity, response, and recovery time toward NO_2 when compared to network structures at RT. This can be attributed to the unique morphology, particle size, efficient adsorption, and desorption of the analyte gas.

Gas-sensing mechanism of $LaFeO_3$ is based on the resistance change during the chemical and electronic interactions between the gas and the $LaFeO_3$, which is based on recognition of target gas through the gas−solid interaction that induces an electronic change of the $LaFeO_3$ surface. The oxygen molecules adsorb on the surface of $LaFeO_3$ in the presence of air to form O_2^-, O^-, and O^{2-} ions by trapping electrons from the conduction band. In the atmosphere of NO_2, $LaFeO_3$ captures electrons, leading to the formation of adsorbed NO_2^-(ads) resulting in further increase in resistance. This adsorbed NO_2^-(ads) reacts with adsorbed oxygen and gives the following product:

dx.doi.org/10.1021/am503318y | ACS Appl. Mater. Interfaces 2014, 6, 13917−13927

$$NO_2^-(ads) + O_2^-(ads) \rightarrow 2O_2^-(ads) + NO_2(g) \quad (1)$$

The desorption of NO_2 molecules results in the decrease of resistance due to the release of trapped electrons on the $LaFeO_3$ surface. The resistance reaches its initial value after complete desorption. From the above results, a hole accumulation space-charge layer was formed under the surface. The perovskite gas-sensing materials are usually classified as p-type (dominated by holes) according to the variation tendency of conductance upon exposure to reducing or oxidizing gases.[43−46]

Figure 12 illustrates the exposure of $LaFeO_3$ thin films to the oxidization gas NO_2; here a different process is envisioned. In this case, the NO_2 molecules adsorb on the $LaFeO_3$ surface acting as acceptors. With an unpaired electron, the NO_2 molecules react with the dangling bond on the $LaFeO_3$ surface, trapping a lone-pair electron of the dangling bond, which results in the formation of free hole. The following reaction (eq 2) takes place on the surface of the film:

$$\begin{aligned} &LaFeO_3 + NO_{2(gas)} \\ &\Leftrightarrow LaFeO_3{-}NO_{2(ads)} \\ &\Leftrightarrow LaFeO_3^+{-}NO_{2(ads)}^- \\ &\Leftrightarrow LaFeO_3{-}NO_{2(ads)} + h \end{aligned} \quad (2)$$

Hence, the increase in concentration of holes dramatically enlarged the band bending while simultaneously decreasing the sensor resistance. In addition to this, it has been reported that higher crystallization and well-defined morphologies can usually lead to enhanced gas-sensing behavior by oxidation of Fe(III), producing Fe(II) complex on the surface of thin films. Meanwhile, $LaFeO_3$ nanostructure thin film samples have more adsorbed oxygen or oxygen in the hydroxyl group as confirmed by the XPS results.

4. CONCLUSION

In summary, different morphologies of nanocrystalline $LaFeO_3$ thin films have been successfully fabricated through RF magnetron sputtering deposition with optimized parameters. Morphology, structure, and surface roughness measurements of the prepared samples confirmed the purity, crystallinity, and phase of the network and nanocube $LaFeO_3$ thin films. The XPS analysis indicated that a large amount of oxygen vacancies appearing on the surface directly contributed to the sensor response. The gas-sensing tests exhibited that the nanocube $LaFeO_3$ thin films possessed high sensitivity, fast response−recovery time, excellent repeatability, and good selectivity to 1 ppm level of NO_2 at RT as compared to the network $LaFeO_3$ thin films, which is mainly attributed to their morphology, particle size, and the numerous surface active sites. Furthermore, the results suggest that the prepared $LaFeO_3$ thin films with excellent surface active sites are a promising candidate for good performance NO_2 gas sensor.

AUTHOR INFORMATION

Corresponding Author

*Phone: +55 (16) 33739828. Fax: +55 (16) 33739824. E-mail: sthirumalairajan@gmail.com.

Notes

The authors declare no competing financial interest.

ACKNOWLEDGMENTS

S.T. gratefully acknowledges the Jawaharlal Nehru Memorial Fund for Doctoral studies (ref: SU-A/270/2011-2012/388 dated 09-12-2010) and also Brazilian research financing institutions CAPES, FAPESP/CEPID 2013/19049-0, INCTMN/CNPq, and FAPESP for financial aid.

REFERENCES

(1) Vander Wal, R. L.; Berger, G. M.; Kulis, M. J.; Hunter, G. W.; Xu, J. C.; Evans, L. Synthesis Methods, Microscopy Characterization and Device Integration of Nanoscale Metal Oxide Semiconductors for Gas Sensing. *Sensors* **2009**, *9*, 7866−7902.

(2) Neri, G.; Bonavita, A.; Galvagno, S.; Siciliano, P.; Capone, S. CO and NO_2 Sensing Properties of Doped-Fe_2O_3 Thin Films Prepared by LPD. *Sens. Actuators, B* **2002**, *82*, 40−47.

(3) Qin, Y.; Li, X.; Wang, F.; Hu, M. Solvothermally Synthesized Tungsten Oxide Nanowires/Nanorods for NO_2 Gas Sensor Applications. *J. Alloys Compd.* **2011**, *509*, 8401−8406.

(4) Joshi, R.; Gomez, H.; Alvi, F.; Kumar, A. Graphene Films and Ribbons for Sensing of O_2, and 100 ppm of CO and NO_2 in Practical Conditions. *J. Phys. Chem. C* **2010**, *114*, 6610−6613.

(5) Afzal, A.; Cioffi, N.; Sabbatini, L.; Torsi, L. NO_x Sensors Based on Semiconducting Metal Oxide Nanostructures: Progress and Perspectives. *Sens. Actuators, B* **2012**, *171−172*, 25−42.

(6) Choi, S. W.; Jung, S. H.; Kim, S. S. Significant Enhancement of the NO_2 Sensin Capability in Networked SnO_2 Nanowires by Au Nanoparticles Synthesized via γ-Ray Radiolysis. *J. Hazard. Mater.* **2011**, *193*, 243−248.

(7) Balazsi, C.; Sedlackova, K.; Llobet, E.; Ionescu, R. Novel Hexagonal WO_3 Nanopowder with Metal Decorated Carbon Nanotubes as NO_2 Gas Sensor. *Sens. Actuators, B* **2008**, *133*, 151−155.

(8) Anjali, S.; Monika, T.; Gupta, V. Room Temperature Trace Level Detection of NO_2 Gas using SnO_2 Modified Carbon Nanotubes Based Sensor. *J. Mater. Chem.* **2012**, *22*, 23608−23616.

(9) Schedin, F.; Geim, A. K.; Morozov, S. V.; Hill, E. W.; Blake, P.; Katsnelson, M. I.; Novoselov, K. S. Detection of Individual Gas Molecules Adsorbed on Graphene. *Nat. Mater.* **2007**, *6*, 652−655.

(10) Enrico, T.; Shigenori, M.; Genji, O.; Yoshihiko, S.; Yoshiro, S.; Kazuaki, W. NO_2 Sensitive $LaFeO_3$ Thin Films Prepared by r.f. Sputtering. *Sens. Actuators, B* **1995**, *25*, 661−664.

(11) Thirumalairajan, S.; Girija, K.; Hebalkar, N. Y.; Mangalaraj, D.; Viswanathan, C.; Ponpandian, N. Shape Evolution of Perovskite $LaFeO_3$ Nanostructures: A Systematic Investigation on Growth Mechanism, Properties and Morphology Dependent Photocatalytic Activities. *RSC Adv.* **2013**, *3*, 7549−7561.

(12) Rothschild, A.; Tuller, H. L. Gas Sensors: New Materials and Processing Approaches. *J. Electroceram.* **2006**, *17*, 1005−1012.

(13) Hara, T.; Ishiguro, T.; Wakiya, N.; Shinozaki, K. Oxygen Sensitivity of Perovskite Type Dielectric Thin Films. *Mater. Sci. Eng., B* **2009**, *161*, 142−145.

(14) Sahner, K.; Moos, R.; Matam, M.; Tunney, J. J.; Post, M. Hydrocarbon Sensing with Thick and Thin film *p*-Type Conducting Perovskite Materials. *Sens. Actuators, B* **2005**, *108*, 102−112.

(15) Huang, L.; Bassir, M.; Kaliaguine, S. Characters of Perovskite-type $LaCoO_3$ Prepared by Reactive Grinding. *Mater. Chem. Phys.* **2007**, *101*, 259−263.

(16) Thirumalairajan, S.; Girija, K.; Ganesh, V.; Mangalaraj, D.; Viswanathan, C.; Ponpandian, N. Novel Synthesis of $LaFeO_3$ Nanostructure Dendrites: A Systematic Investigation of Growth Mechanism, Properties, and Biosensing for Highly Selective Determination of Neurotransmitter Compounds. *Cryst. Growth Des.* **2013**, *13*, 291−302.

(17) Thirumalairajan, S.; Girija, K.; Ganesh, I.; Mangalaraj, D.; Viswanathan, C.; Ponpandian, N. Controlled Synthesis of Perovskite $LaFeO_3$ Microsphere Composed of Nanoparticles via Self-Assembly Process and their Associated Photocatalytic Activity. *Chem. Eng. J.* **2012**, *209*, 420−428.

(18) Fergus, J. Perovskite for Semiconductor-Based Gas Sensors. *Sens. Actuators, B* **2007**, *123*, 1169−1179.
(19) Krupicka, E.; Reller, A.; Weidenkaff, A. Morphology of Nanoscaled $LaMO_3$ Particles (M = Mn, Fe, Co, Ni) Derived by Citrate Precursors in Aqueous and Alcoholic Solvents. *Cryst. Eng.* **2002**, *5*, 195−202.
(20) Song, P.; Qi, W.; Yang, Z. CO-Sensing Characteristics of $La_{0.8}Pb_{0.2}Fe_{0.8}Co_{0.2}O_3$ Perovskite films Prepared by RF Magnetron Sputtering. *Phys. E* **2009**, *41*, 1479−1483.
(21) Le Paven-Thivet, C.; Le Gendre, L.; Le Castrec, J.; Chevire, F.; Tessier, F.; Pinel Prog, J. Oxynitride Perovskite $LaTiO_xN_y$ Thin Films Deposited by Reactive Sputtering. *Solid State Chem.* **2007**, *35*, 299−308.
(22) Enrico, T.; Shigenori, M.; Genji, O.; Yoshihiko, S.; Yoshiro, S.; Kazuaki, W. NO_2 Sensitive $LaFeO_3$ Thin Films Prepared by r.f. Sputtering. *Sens. Actuators, B* **1995**, *25*, 661−664.
(23) Hao, L.; Ling, Y. L.; Hong, T. C.; Zhi, M. L.; Fei, Z. Structural, Chemical, Optical, and Electrical Evolution of SnO_x Films Deposited by Reactive rf Magnetron Sputtering. *ACS Appl. Mater. Interfaces* **2012**, *4*, 5673−5677.
(24) Van Tong, P.; Duc Hoa, N.; Van Quang, V.; Van Duy, N.; Van Hieu, N. Diameter Controlled Synthesis of Tungsten Oxide Nanorod Bundles for Highly Sensitive NO_2 Gas Sensors. *Sens. Actuators, B* **2013**, *183*, 372−380.
(25) You, L.; He, X.; Wang, D.; Sun, P.; Sun, Y. F.; Liang, X. S.; Du, Y.; Lu, G. Y. Ultrasensitive and Low Operating Temperature NO_2 Gas Sensor Using Nanosheets Assembled Hierarchical WO_3 Hollow Microspheres. *Sens. Actuators, B* **2012**, *173*, 426−432.
(26) Tulliani, J. M.; Baroni, C.; Lopez, C.; Dessemond, L. New NO_x Sensors Based on Hematite Doped with Alkaline and Alkaline-Earth Elements. *J. Eur. Ceram. Soc.* **2011**, *31*, 2357−2364.
(27) Su, P. G.; Pan, T. T. Fabrication of a Room-Temperature NO_2 Gas Sensor Based on WO_3 Films and WO_3/MWCNT nanocomposite Films by Combining Polyol Process with Metal Organic Decomposition Method. *Mater. Chem. Phys.* **2011**, *125*, 351−357.
(28) Kaur, J.; Roy, S. C.; Bhatnagar, M. C. Highly Sensitive SnO_2 Thin film NO_2 Gas Sensor Operating at Low Temperature. *Sens. Actuators, B* **2007**, *123*, 1090−1095.
(29) Warang, T.; Patel, N.; Santini, A.; Bazzanella, N.; Kale, A.; Miotello, A. Pulsed Laser Deposition of Co_3O_4 Nanoparticles Assembled Coating: Role of Substrate Temperature to Tailor Disordered to Crystalline Phase and Related Photocatalytic Activity in Degradation of Methylene Blue. *Appl. Catal., A* **2012**, *423*−*424*, 21−27.
(30) Liu, X.; Hu, J.; Cheng, B.; Qin, H.; Jiang, M. Preparation and Gas Sensing Characteristics of p-type Semiconducting $LnFe_{0.9}Mg_{0.1}O_3$ (Ln = Nd, Sm, Gd and Dy) materials. *Curr. Appl. Phys.* **2009**, *9*, 613−617.
(31) Zhang, T.; Liu, L.; Qi, Q.; Li, S.; Lu, G. Development of Microstructure In/Pd-Doped SnO_2 Sensor for Low-Level CO Detection. *Sens. Actuators, B* **2009**, *139*, 287−291.
(32) Zhao, J.; Liu, Y.; Li, X.; Lu, G.; You, L.; Liang, X.; Zhang, T.; Du, Y. Highly Sensitive Humidity Sensor Based on High Surface Area Mesoporous $LaFeO_3$ Prepared by a Nanocasting Route. *Sens. Actuators, B* **2013**, *181*, 802−809.
(33) Czekaj, S.; Nolting, F.; Heyderman, L. J.; Kunze, K.; Kruger, M. Antiferromagnetic Domain Configurations in Patterned $LaFeO_3$ Thin Films. *J. Phys.: Condens. Matter* **2007**, *19*, 386214.
(34) Carotta, M. C.; Butturi, M. A.; Martinelli; Sadaoka, Y. Microstructural Evolution of Nanosized $LaFeO_3$ Powders from the Thermal Decomposition of a Cyano-Complex for Thick Film Gas Sensors. *Sens. Actuators, B* **1997**, *44*, 590−594.
(35) Su, H.; Jing, L.; Shi, K.; Yao, C.; Fu, H. Synthesis of Large Surface area $LaFeO_3$ Nanoparticles by SBA-16 Template Method as High Active Visible Photocatalysts. *J. Nanopart. Res.* **2010**, *12*, 967−975.
(36) Rida, K.; Benabbas, A.; Bouremmad, F.; Pena, M. A.; Sastre, E.; Martinez, A. Effect of Calcination Temperature on the Structural Characteristics and Catalytic Activity for Propene Combustion of Sol−Gel Derived Lanthanum Chromite Perovskite. *Appl. Catal., A* **2007**, *327*, 173−179.
(37) Mickevicius, S.; Grebinskij, S.; Bondarenka, V.; Vengalis, B.; Sliuziene, K. Investigation of Epitaxial $LaNiO_{3-x}$ Thin Films by High-Energy XPS. *J. Alloys Compd.* **2006**, *423*, 107−111.
(38) Kim, H. J.; Lee, J. H. Highly Sensitive and Selective Gas Sensors Using *p*-Type Oxide Semiconductors: Overview. *Sens. Actuators, B* **2014**, *192*, 607−627.
(39) Barreca, D.; Bekermann, D.; Comini, E.; Devi, A.; Fischer, R. A.; Gasparotto, A.; Maccato, C.; Sada, C.; Sberveglieri, G.; Tondello, E. Urchin-Like ZnO Nanorod Arrays for Gas Sensing Applications. *CrystEngComm* **2010**, *12*, 3419−3421.
(40) Russo, N.; Mescia, D.; Fino, D.; Saracco, G.; Specchia, V. N_2O Decomposition over Perovskite Catalysts. *Ind. Eng. Chem. Res.* **2007**, *46*, 4226−4231.
(41) Law, M.; Kind, H.; Messer, B.; Kim, F.; Yang, P. Photochemical Sensing of NO_2 with SnO_2 Nanoribbon Nanosensors at RT. *Angew. Chem., Int. Ed.* **2002**, *41*, 2405−2408.
(42) Qin, Y.; Hu, M.; Zhang, J. Microstructure Characterization and NO_2-Sensing Properties of Tungsten Oxide Nanostructures. *Sens. Actuators, B* **2010**, *150*, 339−345.
(43) Galatsis, K.; Cukrov, L.; Wlodarski, W.; McCormick, P.; Kalantar-zadeh, K.; Comini, E. G. *p*- and *n*-type Fe-doped SnO_2 Gas Sensors Fabricated by the Mechanochemical Processing Technique. *Sens. Actuators, B* **2003**, *93*, 562−565.
(44) Gurlo, A.; Barsan, N.; Oprea, A.; Sahm, M.; Sahm, T.; Weimar, U. An *n*- to *p*-type Conductivity Transition Induced by Oxygen Adsorption on α-Fe_2O_3. *Appl. Phys. Lett.* **2004**, *85*, 2280−2282.
(45) Wang, S.; Zhang, H.; Wang, Y.; Wang, L.; Gong, Z. Facile One-pot Synthesis of Au Nanoparticles Decorated Porous α-Fe_2O_3 Nanorods for *in situ* Detection of VOCs. *RSC Adv.* **2014**, *4*, 369−373.
(46) Sorita, R.; Kawano, T. A Highly Selective CO Sensor using $LaMnO_3$ Electrode- Attached Zirconia Galvanic Cell. *Sens. Actuators, B* **1997**, *40*, 29−32.